IN-02-CR
243105
30P.

NUMERICAL INVESTIGATIONS IN THREE-DIMENSIONAL INTERNAL FLOWS

SEMI-ANNUAL STATUS REPORT

1 JANUARY THROUGH 30 JUNE 1989
(GRANT INACTIVE 1 OCTOBER 1988 TO 31 DECEMBER 1988)

Prepared for:

NASA-AMES RESEARCH CENTER

MOFFETT FIELD, CA 94035

UNDER NASA GRANT

NCC 2-507

by:

WILLIAM C. ROSE

ENGINEERING RESEARCH AND DEVELOPMENT CENTER

UNIVERSITY OF NEVADA, RENO

RENO, NV 89557

UNR SEMI-ANNUAL STATUS REPORT
1 JANUARY THROUGH 30 JUNE 1989

The attached technical report is a written version of the technical paper presented at the 6th National Aero-Space Plane Technical Symposium held at the Naval Postgraduate School, Monterey, CA 24-28 April 1989. This report is being substituted for and constitutes the Semi-Annual Status Report.

OBJECTIVES (U)

(U) DEVELOP AN UNDERSTANDING OF FLOW FIELDS THAT EXIST IN SIDEWALL COMPRESSION (SWC) INLET MODELS.

- TESTED IN FREESTREAM AND WITH THICK ENTERING BOUNDARY LAYERS.

(U) ESTABLISH CAUSE-AND-EFFECT RELATIONSHIPS BETWEEN INLET GEOMETRY, ENTERING CONDITIONS, AND RESULTANT FLOW FIELDS.

- SWC FLOW FIELDS ARE HIGHLY THREE-DIMENSIONAL AND ARE NON-INTUITIVE.
- REQUIRED BEFORE SYSTEMS CAN BE "DESIGNED."

(U) COMPARE NUMERICAL SIMULATIONS WITH THE LIMITED DATA AVAILABLE TO DATE.

- AID IN AN UNDERSTANDING OF BOTH THE SIMULATIONS AND THE EXPERIMENTS.
- CODE STRENGTHS AND WEAKNESSES.

APPROACH (U)

(U) USE AN EXPLICIT, TIME-ACCURATE FULL NAVIER-STOKES (FNS) CODE FOR BOTH LAMINAR AND TURBULENT (BALDWIN-LOMAX) BOUNDARY LAYERS TO NUMERICALLY SIMULATE SWC INLET MODEL FLOW FIELDS.

(U) EXAMINE THESE SIMULATIONS AS THEY ARE INFLUENCED BY:

- MACH NUMBER
- CHANGES IN SIDEWALL COMPRESSION ANGLE
- HYPERSONIC VISCOUS INTERACTION EFFECTS
- THICK ENTERING BOUNDARY LAYERS.

The schematic representation of the sidewall compression inlet shows the sidewalls swept back at 30° starting at the leading edge of the ramp towards the cowl. The cowl is shown positioned with its lip at the entrance to the constant area throat section. The ramp and cowl are identified. This inlet has 6° sidewall compression angles and was tested by Trexler, et al. in the freestream, that is with no entering boundary layer, at the 2 tunnel test conditions indicated. The numerical simulation was carried out for these entering conditions under the assumption that all of the boundary layers were laminar and existed from the leading edge of each solid surface. Primary results from the numerical simulation are depicted here on the vertical center plane, which is 21 of 41, and the horizontal center plane, which is number 31 of 61. Since the numerical simulation is a full three-dimensional viscous simulation, information is also available at other planes and is depicted in this presentation on certain selected cross flow planes, in addition to the 2 orthogonal planes indicated here. There are 63 cross-flow planes within the inlet.

FREESTREAM CASE (U)

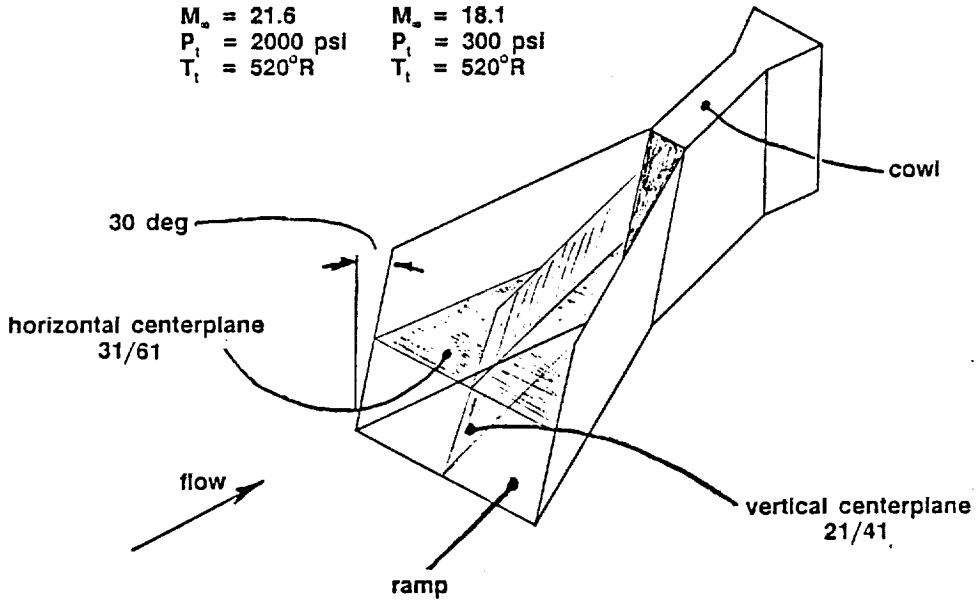

all laminar boundary layers

This figure shows the Mach number contours obtained for a freestream case at a Mach number of 18.1 with a geometric contraction ratio (GCR) equal to 4.0. The cowl is in the aft position, that is at the entrance to the constant area section. Information on the vertical center plane is shown here to an expanded vertical scale which distorts the indicated angularity but allows details of the solution to be exhibited. The ramp surface is located near the top while the cowl is on the lower surface. The sidewalls sweep back angle of 30° is indicated. The sidewalls are the only geometric compressing surfaces in the inlet. They generate a pair of intersecting shock waves that form a large discontinuity on the vertical center plane and cause a large pressure rise to be felt on the ramp surface. Later these shock waves are transmitted and interact with the sidewall boundary layers and, again, reflect and intersect on the center plane at the position indicated by the intersecting reflected shocks. This causes a further pressure rise on the ramp boundary layer which separates and evolves forward in the time-dependent numerical simulation. The displacement effects of the separated ramp boundary layer induce a separation shock that is evidenced in the vertical center plane and merges with the intersecting sidewall shocks as depicted. The minimum Mach number in the core of this simulation has a value of approximately 3.5.

MACH NUMBER CONTOURS FOR FREESTREAM CASE (U)

M_∞ = 18.1 6° Sidewalls GCR = 4.0 Cowl Aft

Vertical Center Plane

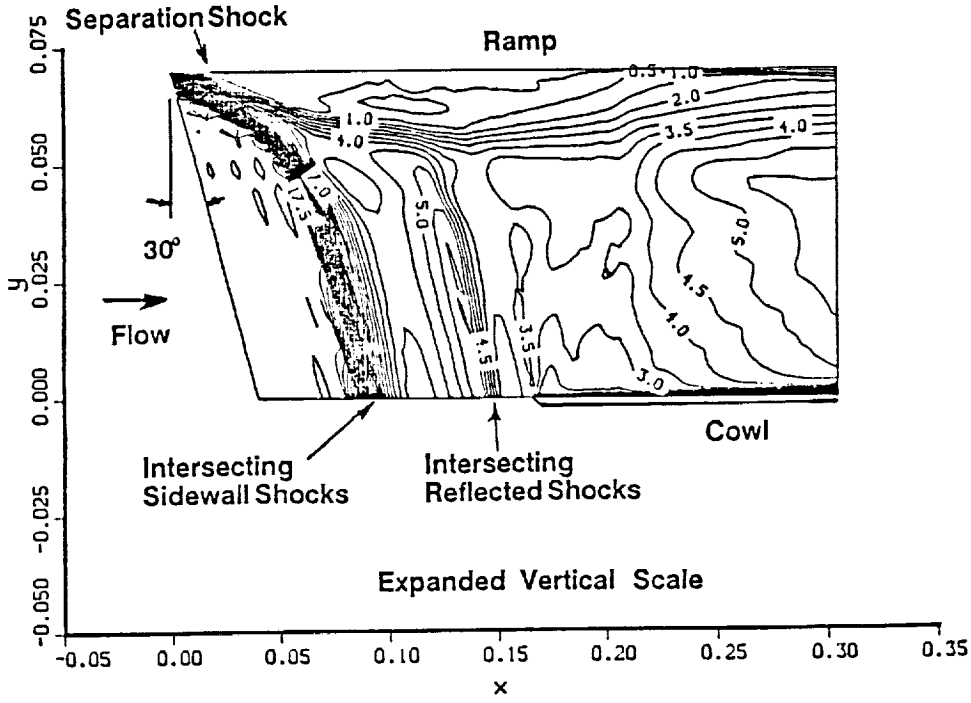

This figure shows the Mach number contours on the horizontal center plane for the case indicated on the previous figure. This horizontal center plane view has an expanded lateral scale to allow depiction of the sidewall shock waves and the sidewall separations resulting from the interaction of the sidewall shock waves and the sidewall's laminar boundary layer. The intersecting sidewall shock waves and the intersecting reflected shock waves are also visible, both occurring well upstream of the entrance to the constant area throat. The design objective of having the sidewall shoulder perform a shock cancellation function is clearly not met in this simulation because the sidewall shock waves strike the sidewalls well upstream of the sidewall shoulders. This is due to the curvature and displacement of the sidewall shock waves due to the hypersonic viscous interaction occurring at the high Mach number for this simulation. In fact, it is evident that the shock cancellation occurs not for the first set of sidewall shock waves, but for the reflected shock waves. This strong effect of viscous interaction is evident for all the simulations conducted in the current study when the freestream Mach number was high.

MACH NUMBER CONTOURS FOR FREESTREAM CASE (U)

M_∞ = 18.1 6° Sidewalls GCR = 4.0 Cowl Aft

Horizontal Center Plane

Expanded Lateral Scale

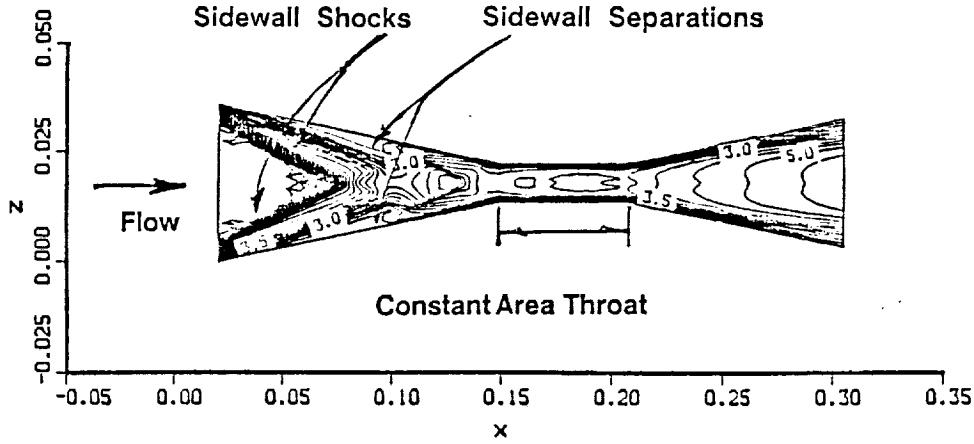

This figure shows Mach number contours for both the vertical and horizontal center planes for the geometric contraction ration equal to 5.0 and a freestream Mach number of 21.6. The general nature of the flow is similar to that discussed in the previous two figures. However, for the higher Mach number and higher contraction ratio, stronger shock waves and higher pressure rises exist in the inlet, causing the ramp boundary layer to separate, in this simulation, all the way to the leading edge of the ramp, producing a very strong, oblique separation shock wave that dominates the behavior of the flow on the ramp side of the inlet. At the horizontal center plane, this separation shock appears as a nearly nominal shock connecting the primary sidewall oblique shocks. Very large turning angles exist across this strong wave system. Information obtained for the Mach number contours and velocity vectors will be portrayed at the selected four cross flow planes to demonstrate the nature of the three dimensional flow field obtained from the simulations.

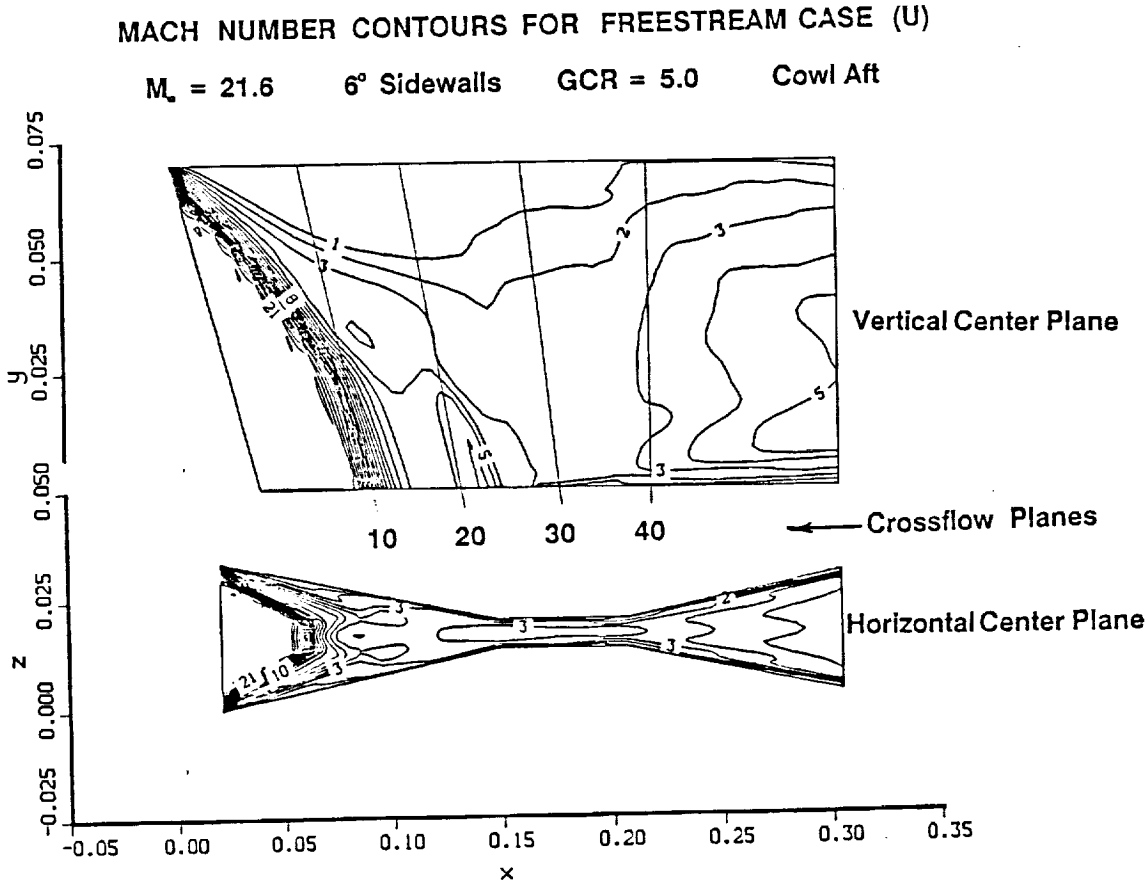

This figure shows the Mach number contours for the flow simulation carried out at Mach 21.6 discussed in the previous figure. Cross flow planes of 10, 20, 30 and 40 are shown and are referenced to the calculation planes indicated on the previous figure. Calculation plane 10 is immersed in the sidewall flow field and is strongly dominated by the separated ramp boundary layer and its associated low Mach number regions. A highly distorted three-dimensional flow is observed. This distortion is carried beyond that and downstream of the sidewall boundary layer reattachment, the sidewall boundary layers are observed to be much compressed, although a large separation region is still evident on the ramp. This highly distorted flow and attendant low momentum associated with the ramp flow field continues throughout the remainder of the solution, while the sidewall boundary layers and the cowl boundary layer grow in the downstream direction.

MACH NO. CONTOURS FOR FREESTREAM CASE (U)

M_∞ = 21.6 6° Sidewalls GCR = 5.0 Cowl Aft

Cross Flow Planes

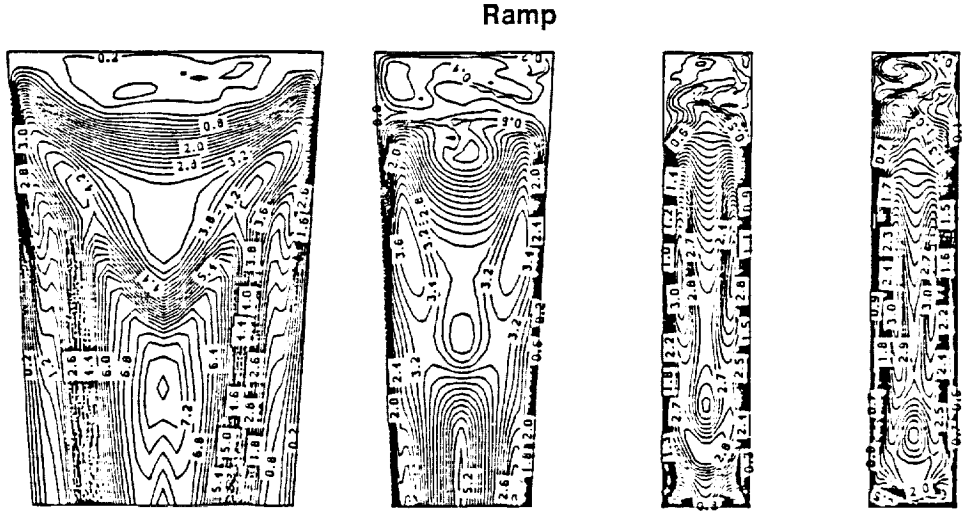

This figure depicts the velocity vectors for the Mach 21.6 case discussed in the previous two figures. In the vertical center plane, the effects of the large separation (including back flow that persists nearly to the leading edge of the inlet) and the highly distorted flow field resulting from its displacement effects are clearly seen. In the horizontal center plane, the flow angularity associated with the sidewall shock wave structure is evident. This plane shows only a limited number of vectors and details are not evident in this plot. The following figure shows the level of detail available in the present simulation.

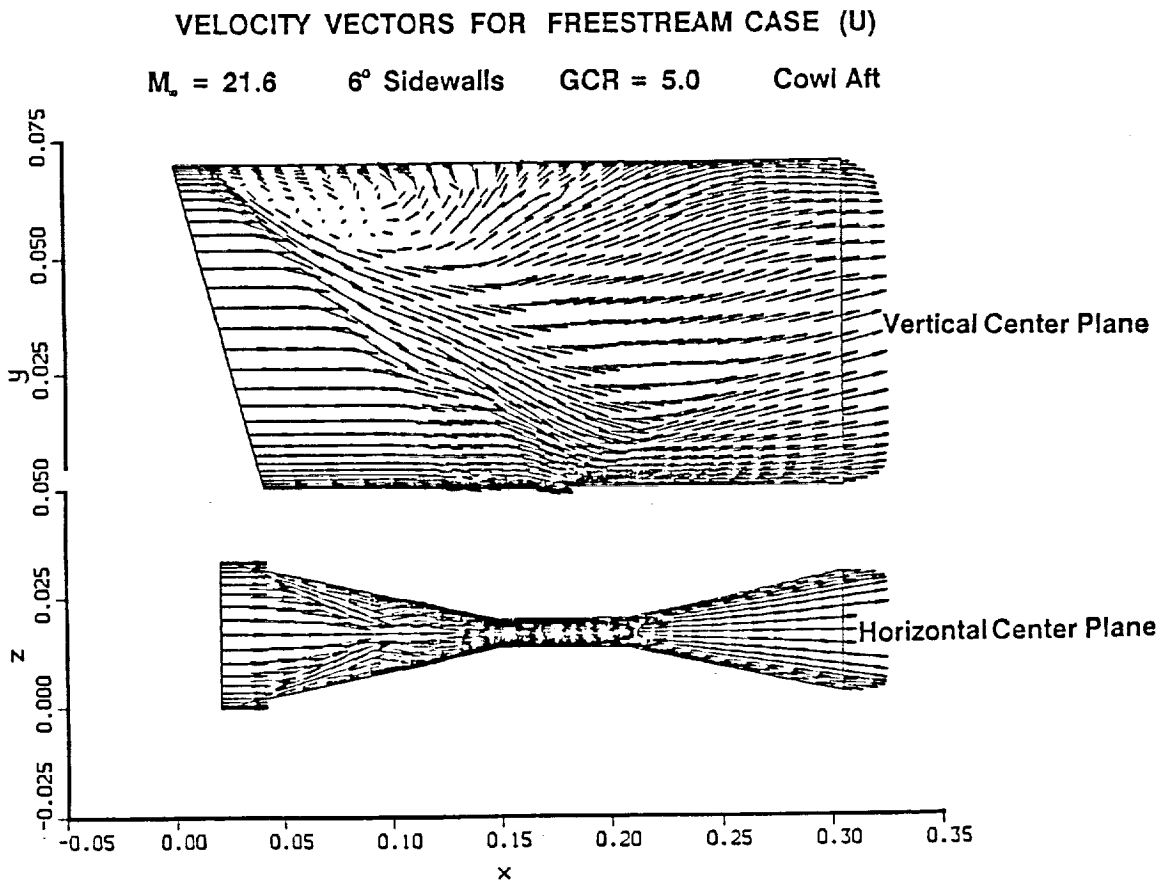

This figure shows an enlarged velocity vector plot at a plane above the cowl but below the horizontal center plane. It shows the behavior of a representative velocity vector field just ahead of the entrance to the throat. It is clear that a well resolved laminar separation region and its associated displacement effects exist.

ENLARGED VELOCITY VECTOR PLOT (U)

Plane Above Cowl Just Ahead of Throat

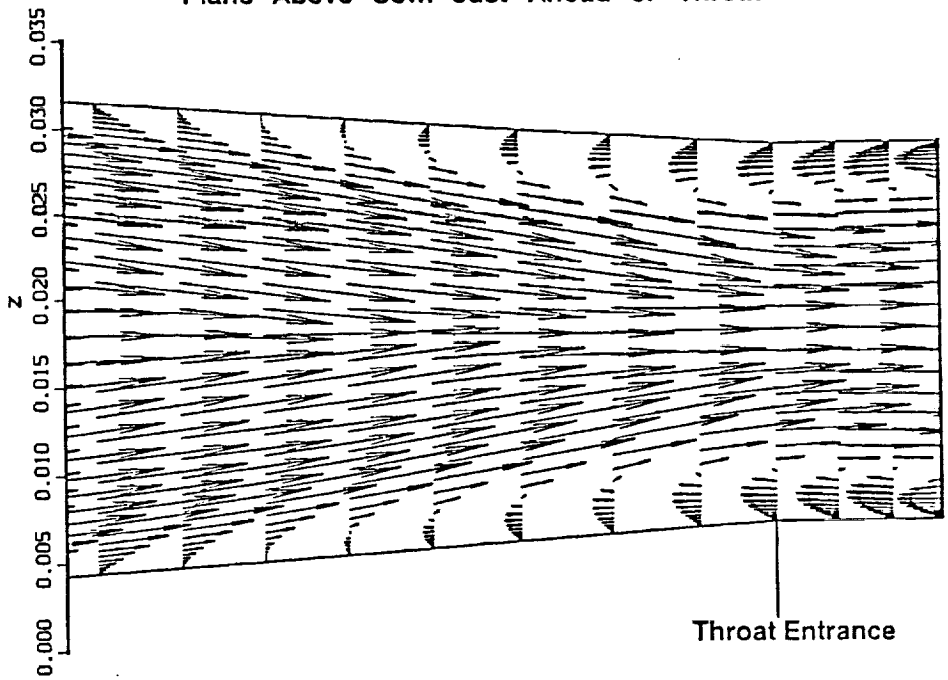

Velocity vectors on the four representative cross flow planes discussed previously are shown in this figure. The large lateral flow that represents convergence of the flow in the upstream portion near the ramp surface and a large flow along the direction of sweep on the sidewalls leading to a large spillage. Just after the cowl is encountered (Station 30), large flow angles toward the cowl surface are evident and result in a partial stagnation of the flow at the cowl surface leading to very high pressures in that region.

VELOCITY VECTORS FOR FREESTREAM CASE (U)

M_∞ = 21.6 6° Sidewalls GCR = 5.0 Cowl Aft

Cross Flow Planes

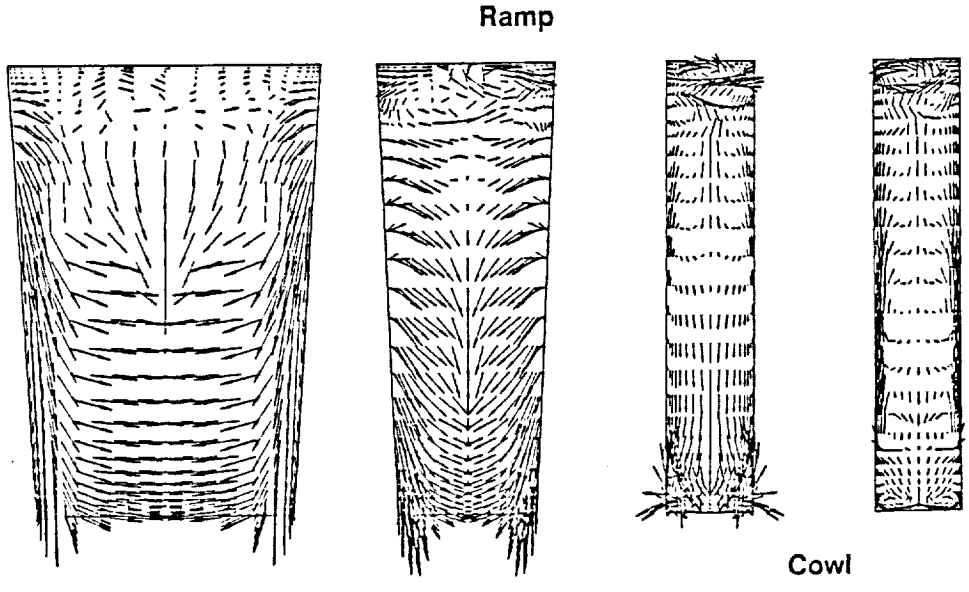

The results of the simulations depicted in the previous figures are entertaining and suggest the nature of the challenging, fully three-dimensional flow fields that one encounters in sidewall compression inlets. However, the validity of these simulations needs to be established. Limited experimental surface pressure distributions were obtained in the studies by Trexler, et al., but no flow field information was obtained. This figure shows a comparison for the ramp surface pressure distributions obtained at a freestream Mach number of 21.6 for two different geometric contraction ratios of 5.0 and 4.0. For the 4.0 case, the pressures in the upstream region are under-predicted by the code, but the pressure rise is located at approximately the right streamwise station and is somewhat over-predicted by the simulation within the constant area throat section. For the 5.0 case, the simulation over-predicts the pressure rise in both the upstream region and within the constant area throat, however, the pressure rises do occur at approximately the same locations. The simulation predicts a separation that extends all the way to the leading edge of the inlet, producing an even stronger viscous interaction with an attendant high surface pressure. The upstream experimental pressures for both the 4.0 and 5.0 cases are substantially above any pressures that could be expected on the basis of an attached laminar boundary layer, indicating the large upstream influence of the ramp separation. The much higher pressures are predicted in the numerical simulation, but the details differ from those of the experiment.

COMPARISON OF EXPERIMENTAL AND NUMERICAL SURFACE PRESSURE DISTRIBUTIONS (U)

M_∞ = 21.6 6° Sidewalls Freestream Case

Ramp Centerline

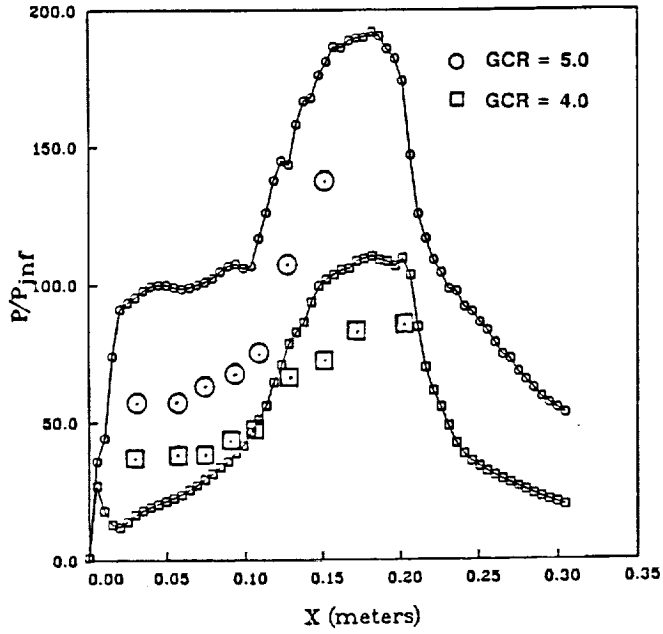

This figure shows the surface pressure distributions for the sidewall center line for the same two contraction ratios as shown in the previous figure. Although the data are very limited, the simulations appear to predict the seemingly implausible variations in the surface pressures. Again, the apparently high pressures near the sidewall leading edge are reasonably well predicted. This and the previous figure indicate that the simulations do a reasonable job of providing some quantitative details and that the qualitative nature of the flows is certainly correct.

COMPARISON OF EXPERIMENTAL AND NUMERICAL SURFACE PRESSURE DISTRIBUTIONS (U)

M_∞ = 21.6 6° Sidewalls Freestream Case

Sidewall Centerline

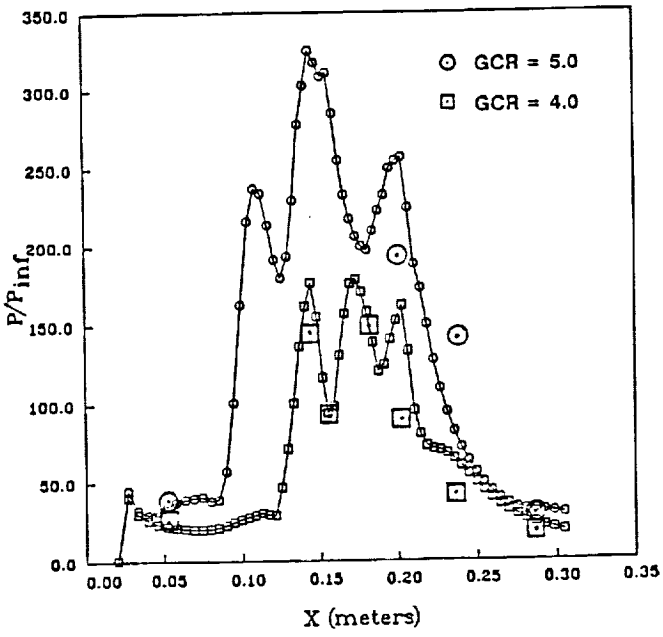

This figure shows the predicted surface pressure distribution on the cowl center line. No experimental data are available for this location, however, the simulations alone are worthy of discussion. The surface pressures are shown all along the entire lower surface of the calculation, including the region upstream of the cowl lip station. As would be expected, significant pressure rises are observed upstream of the cowl lip due to the pressure rise associated with the intersection of the sidewall shock waves, and, in the case of the 5.0 GCR, yet another intersection of the reflected sidewall shocks is seen. Relief of these pressure rises occurs upstream of the cowl lip station along the simulation's outflow boundary. In contrast, substantial pressure rises exist on the cowl. A pressure ratio of about 1500 is seen for the GCR = 5.0 and approximately 300 for the GCR = 4.0.

NUMERICAL SURFACE PRESSURE DISTRIBUTION (U)

M_∞ = 21.6 6° Sidewalls Freestream Case

Cowl Centerline

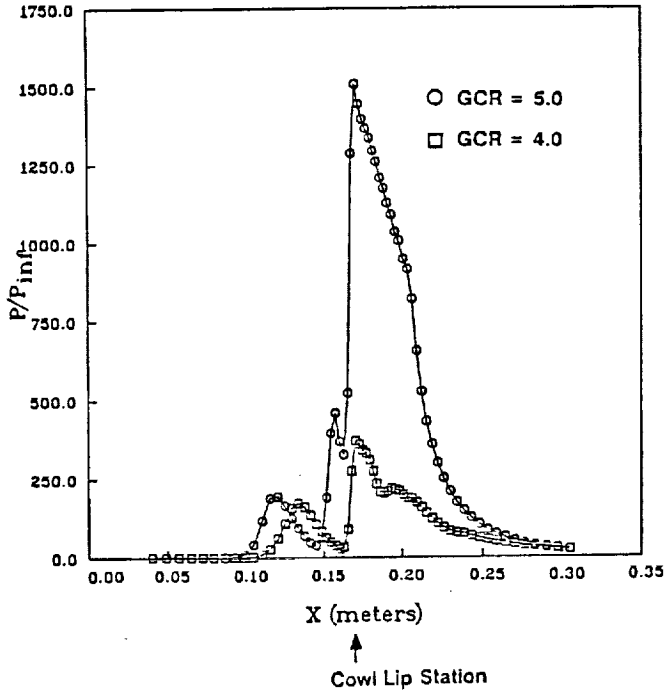

In an attempt to better understand the nature of the disagreement between the simulation and the experiment for the GCR equal to 5.0 case at Mach 21.6 discussed earlier, the time evolution of the surface pressure on the ramp center line was plotted at several different time levels. Early in the solution, at a body time (BT), that is, the number of inlet lengths traversed at the freestream velocity, equal to 1.8, the hypersonic viscous interaction pressure rise and decay is clearly seen, and an upstream influence of the separating laminar boundary layer is evident in the development. At BT = 6.4, the surface pressure distribution is indicating a characteristic laminar separation plateau and pressure rise ahead of the constant area throat. Between 6.4 and 10.5 the experimental data agree fairly well with the simulation. Beyond 10.5 a minor increase in boundary layer displacement effects produced the additional 30% increase in pressure. No significant further evolution of the solution occurred beyond 17.8. The simulations are correct in that they contain a separated ramp boundary layer and produce significant pressure rises well above those that could be expected for an attached flow. Early attempts to simulate this flow, running the usual calculation time of about between 2 and 3 indicated very low pressures and led to the suspicion concerning the experimental data, however, it now appears that the experimental data are probably correct. The reason for the apparently long required computation times when large separation effects are present appears to be related to the fact that the characteristic velocity for development is the separation and circulation velocity and is no longer related to the freestream velocity. This situation appears to prolong the required calculation time by up to a factor of 5 in order to achieve convergence for the time dependent simulation.

TIME EVOLUTION OF NUMERICAL SURFACE PRESSURE DISTRIBUTION (U)

M_∞ = 21.6 6° Sidewalls Freestream Case

Ramp Centerline

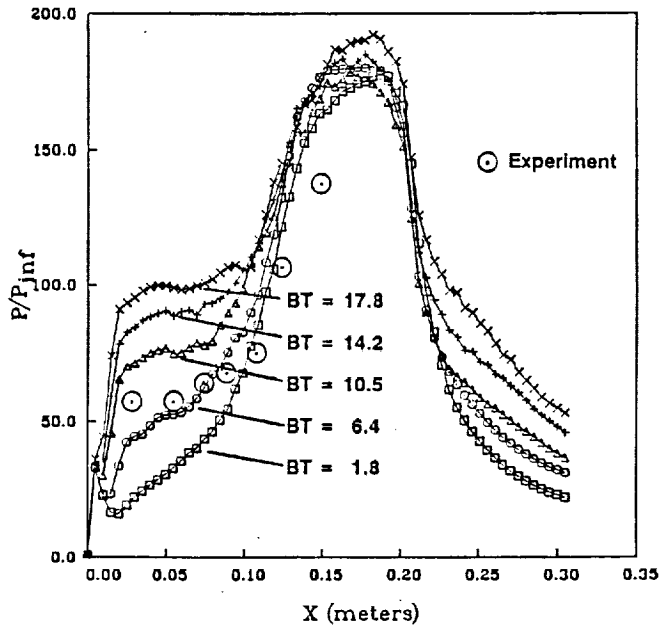

This figure shows a time evolution of the sidewall center line surface pressure distribution for the same case as discussed in the previous figure. Nominal agreement with the very limited experimental data is seen, and in particular, the somewhat higher pressure ratio (a value near 40 times freestream) near the leading edge is in agreement with the final numerical simulation value. This high pressure results from the upstream influence of the shock wave induced laminar separations on the sidewalls.

TIME EVOLUTION OF NUMERICAL SURFACE PRESSURE DISTRIBUTION (U)

M_∞ = 21.6 6° Sidewalls Freestream Case

Sidewall Centerline

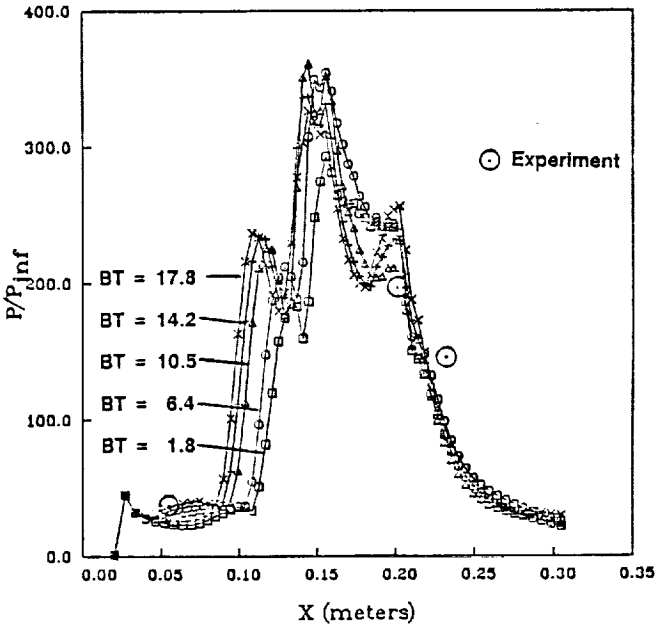

In addition to the simulations discussed previously, all with the cowl positioned at the entrance to the throat, a simulation was carried out that corresponds to a positioning of the cowl tested experimentally, that is at a position 79% of the distance from the sidewall leading edge to the entrance to the throat. Surface pressures on the ramp center line obtained experimentally for the cowl aft position were those discussed previously and are repeated in this figure. The Mach number for this simulation is 18.1 and the geometric contraction ratio is 4.0. When the cowl is positioned in the forward position, the numerical simulation indicates a sudden pressure rise at the inflow to the inlet corresponding to a nearly normal shock wave being taken at the freestream Mach number. An increase in pressure is observed downstream of that pressure rise up to a value of about 250 times freestream pressure. The experiment, on the other hand, appears to represent a different flow condition in the upstream portion of the inlet. Experimentally, higher pressures are observed compared to the retracted cowl case, followed by a rise to approximately the same value as those observed in the numerical simulation. The experimental condition is described by Trexler and Weidner as a "soft unstart," whereas the numerical simulation depicts a "hard unstart." Additional studies are required before differences in the experiment and simulation can be resolved.

COMPARISON OF EXPERIMENTAL AND NUMERICAL
SURFACE PRESSURE DISTRIBUTIONS (U)

M_∞ = 18.1 6° Sidewalls GCR = 4.0 Freestream Case

Ramp Centerline

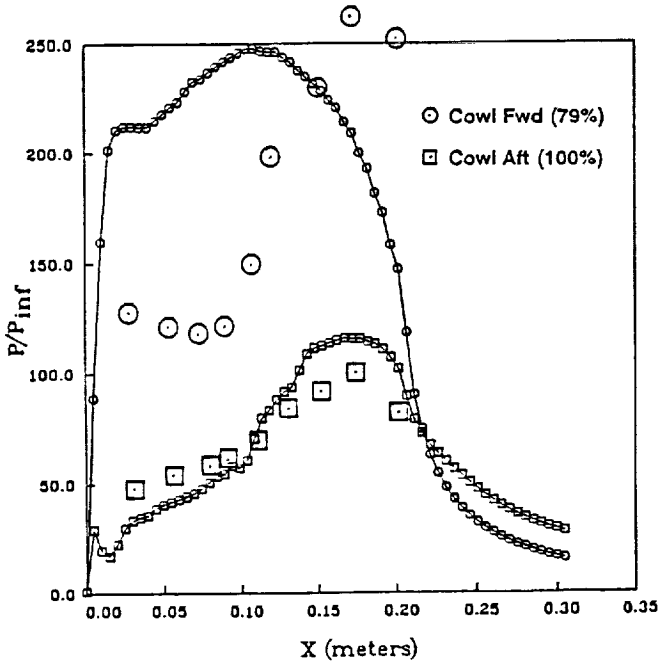

The sidewall center line pressure distribution for the conditions described on the previous figure is shown in this figure. For the case of the cowl aft, the simulations over-predict the pressure rise when compared with the experimental data. However, for the cowl forward, where experimental data are available, the simulation does a reasonably good job of predicting the pressure rises. This simulation supports the concept of an unstarted inlet whose pressure rises are not substantially different from those that would be observed across a normal shock at the freestream Mach number.

COMPARISON OF EXPERIMENTAL AND NUMERICAL SURFACE PRESSURE DISTRIBUTIONS (U)

M_∞ = 18.1 6° Sidewalls GCR = 4.0 Freestream Case

Sidewall Centerline

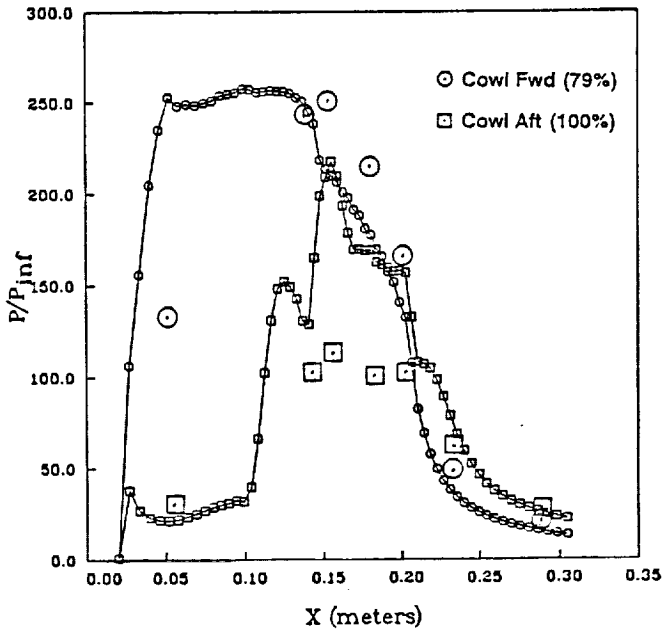

This figure shows the simulated Mach contours on the horizontal center plane in the experimental inlet with the 6 degree sidewall compression angles discussed in the previous figures, and three other hypothetical inlets with reduced sidewall angles of 4, 2 and 0 degrees. For the 6 degree case, the sidewall shock waves are clearly shown and strike the sidewall boundary layer and interact with it, causing a separation that exists well upstream of the entrance to the constant area throat. The pressure rises associated with the sidewall shock waves are sufficient to separate the sidewall boundary layers. An investigation using the hypothetical inlets was carried out to determine whether this extensive separation was due primarily to the effects of strong hypersonic viscous interaction shock reflection or whether the interaction strength could be reduced by reducing the geometric compression angles. The reduction in sidewall angle is not accompanied by a reduction in the extent of laminar separation. With decreasing sidewall angle, the shock wave strength should be substantially reduced, however, since the Mach number downstream of the sidewall shock wave is increasing as the sidewall angle is decreased, the strength of the hypersonic viscous interaction is increased. The combination of decreasing sidewall angle and increasing hypersonic viscous interaction leads to flows in the hypothetical inlets that all contain extensive regions of sidewall separation. Because of the possible effect of grid spacing near the leading edges on hypersonic viscous interaction, these results should be considered preliminary. Additional studies into this effect are underway.

EFFECT OF SIDEWALL COMPRESSION ANGLE (U)
M = 18.1

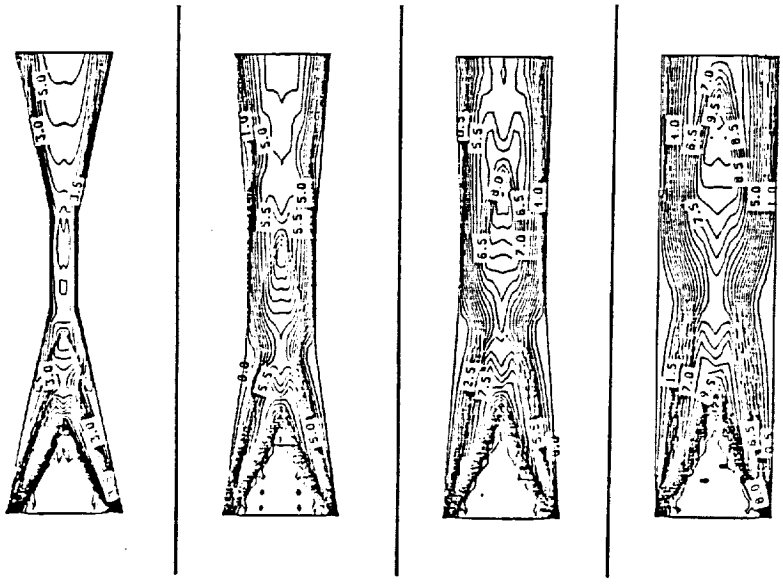

6 4 2 0

Sidewall Angles

This figure shows the surface pressure distribution along the sidewall center line for the four different sidewall angle cases discussed in the previous figure. Pressures have been non-dimensionalized by the observed asymptotic pressure in the simulation, that is the pressure ahead of the effects of the sidewall shock wave interactions but downstream of the region of strong hypersonic viscous interaction. The forward portion of these pressure distributions indicate the large change in the hypersonic viscous interaction effects pointed out in the previous figure, with the 0 degree sidewall angle having the highest pressure rise near the leading edge and the 6 degree having the lowest. When the pressure rises are non-dimensionalized by the asymptotic pressure, the complicated flow field appears to be reduced in complexity somewhat, each distribution demonstrating a recognizable laminar shock wave boundary layer interaction characteristic with an upstream "plateau" followed by a reattachment pressure rise for all of the cases. Even though the flow within these high speed inlets is rather complicated, certain recognizable characteristics of simplified interactions are evident in the simulation.

EFFECT OF SIDEWALL COMPRESSION ANGLE
ON SURFACE PRESSURE DISTRIBUTION (U)

M_∞ = 18.1 Cowl Aft (100%)

Sidewall Centerline

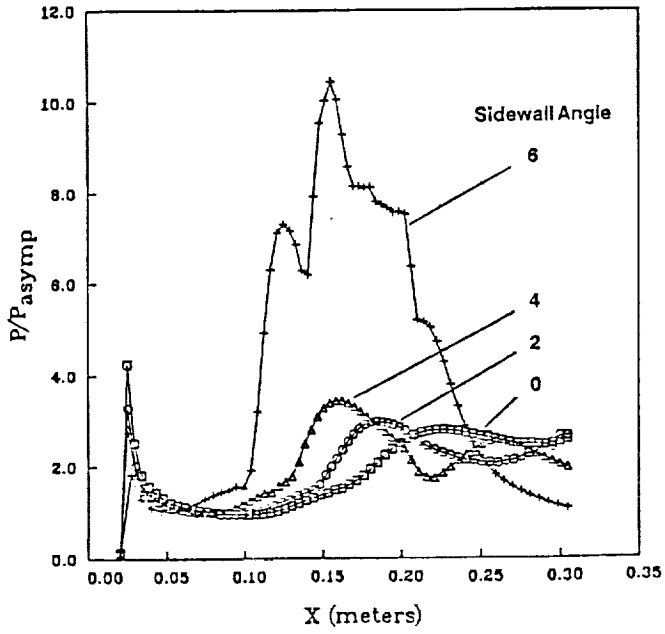

This figure shows the effect of a variation in Mach number on one (4 degree sidewall) of the hypothetical inlets discussed in the previous figure. With a reduction in Mach number from 18.1 to 10, one would expect that the sidewall shock wave angle would increase, causing an interaction with the sidewall boundary layer to occur further upstream than that depicted for the 18.1 case. In contract to that expectation, the interaction for the Mach 10 case occurs downstream within the constant area section. This arises because of the substantially reduced hypersonic viscous interaction, producing less shock curvature and forward displacement of the sidewall shock system allowing the intersection to occur further downstream in the inlet. With a further reduction in the Mach number from 10 to 6, the interaction with the sidewall boundary layers occurs further forward. For the case shown here, an effective cancellation of the sidewall shock system occurs at the sidewall shoulder and no separation results. The pronounced difference between the boundary layer thicknesses evident for each of these cases is clearly seen.

EFFECT OF MACH NUMBER ON 4 DEGREE SIDEWALL CASE (U)

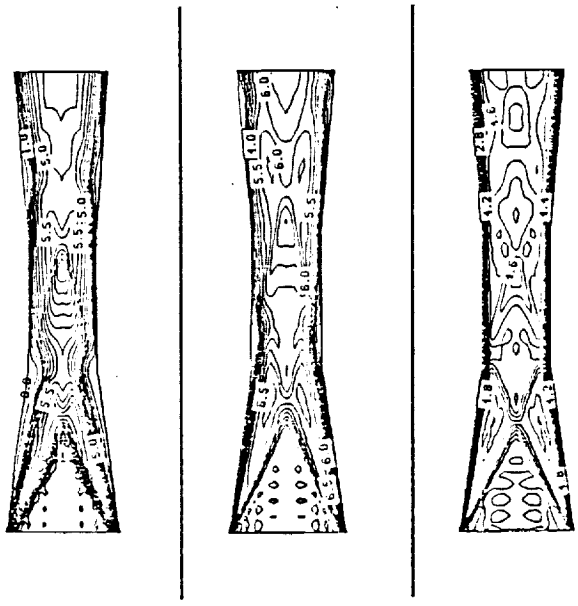

18.1 10.0 6.0

Mach Number

This figure shows a schematic of the second experimental arrangement studied numerically in the present investigation. A sidewall compression inlet (the geometric compression ratio of 5.0, 30 degree sweep, 6 degree sidewall compression angle) was mounted approximately 1.6 meters downstream of the leading edge of a 4 degree wedge and was run in helium at a Mach number of 17.7. A shock wave from the wedge reduces the Mach number from 17.7 to approximately 11.5 and the laminar boundary layer that develops on the wedge undergoes a natural transition at about 0.9 meters. This transition was simulated instantaneously in the code, providing a turbulent boundary layer entering the inlet whose thickness is approximately equal to one-third of the cowl height. In the simulation, the boundary layer on the cowl and sidewalls above the turbulent boundary layer were assumed to be laminar.

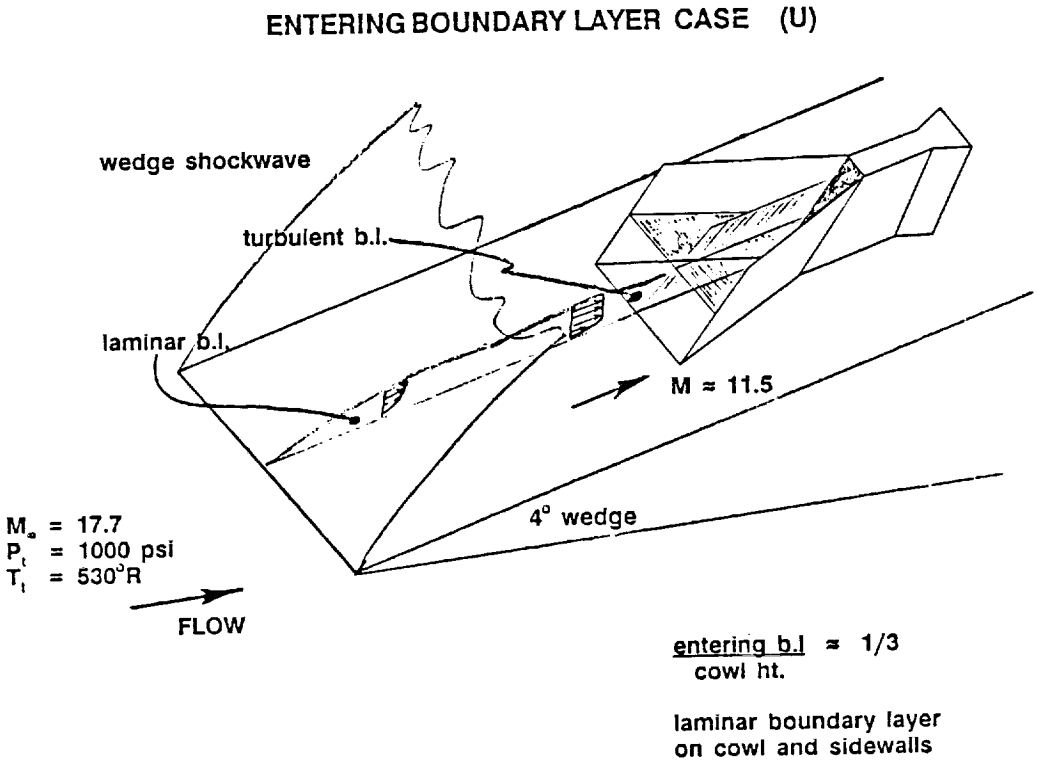

This figure shows the Mach number contours for the compression ratio 5.0 inlet placed on the 4 degree wedge with the entering turbulent boundary layer. The freestream Mach number is 17.7. Only a portion of the entire numerical simulation is shown between approximately 1.3 and 1.9 meters. The entering turbulent boundary layer can be seen in the upper portion of the figure which shows the Mach number contours for the vertical center plane. The position of the inlet ramp leading edge and the cowl are shown. The local Mach number, in the absence of the effects of the turbulent boundary layer entering the inlet, has a value of approximately 11.5. The sidewall shock waves, however, cause a pressure rise that separates the ramp's boundary layer and causes a large upstream influence, approximately equal to the length of the inlet. This thickening turbulent boundary layer produces an additional unexpected oblique shock wave that further reduces the Mach number from 11.5 to approximately 8. To stabilize the upstream propagation of the separation, 0.3% of the captured mass flow was removed from the ramp boundary layer. The flow shown here is for a steady solution obtained with a cowl in the full aft position (100%). The Mach number contours on the horizontal center plane are also shown in this figure and indicate the separation shock wave and a pair of sidewall shock waves whose angle is substantially increased due to the encroachment of the turbulent boundary layer flow.

MACH NO. CONTOURS FOR ENTERING BOUNDARY LAYER CASE (U)

M_∞ = 17.7 6° Sidewalls GCR = 5.0 Cowl Aft (100%)

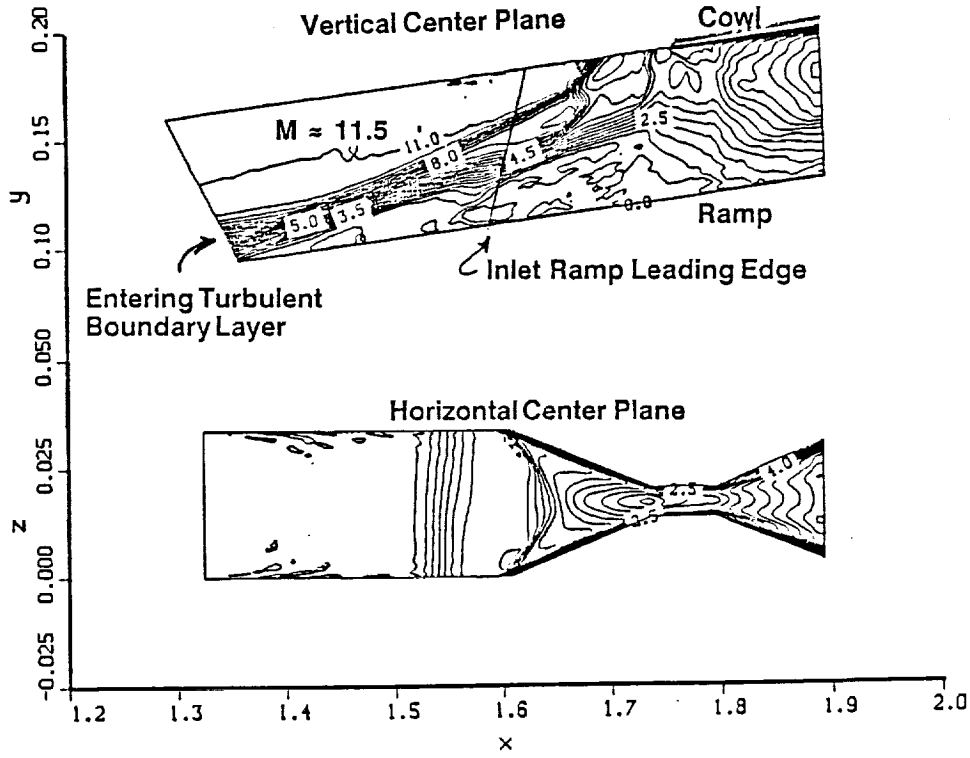

The rather unexpected nature of the flow field shown on the previous figure can be confirmed by examining the surface pressure distribution taken along the ramp center line as shown in this figure in comparison with the experimental data. The pressure rises of approximately 12 to 15 on the ramp upstream of the inlet indicated by the experimental data and in nominal agreement with the pressure rises observed in the simulation confirm the simulation's prediction of a substantial upstream influence propagating through the wedge boundary layer. Since the values of the pressure rise are about the same, one would infer that the strength of the additional oblique shock wave observed is probably correct. The experimental pressure distribution indicates even a further upstream extent of the pressure rises due to the sidewall shock wave system, indicating that the Mach contours shown on the previous slide are certainly qualitatively correct. A higher experimental pressure rise is observed than in the simulation, possibly due to the compression on the ramp occurring at a somewhat higher Mach number than indicated in the simulation.

COMPARISON OF EXPERIMENTAL AND NUMERICAL SURFACE PRESSURE DISTRIBUTIONS (U)

M_∞ = 17.7 6° Sidewalls GCR = 5.0 Wedge Case

Ramp Centerline

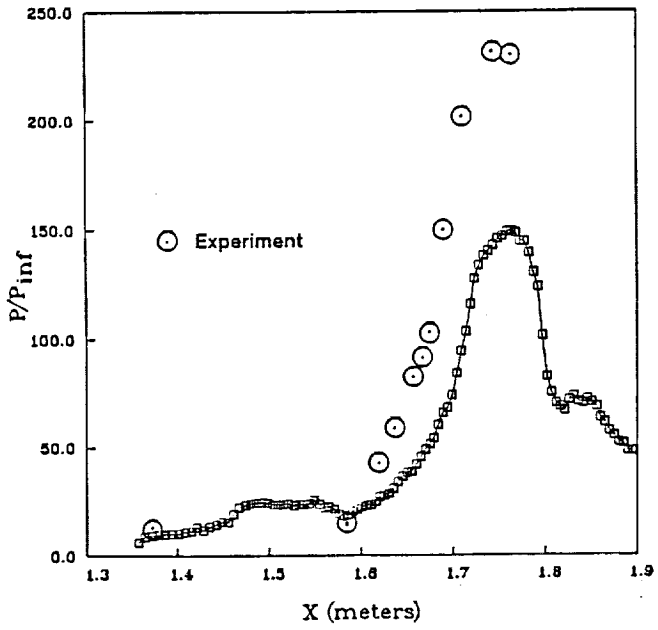

Pressure distributions along the sidewall center line are shown in this figure. Over most of the inlet, the experimental pressure distributions are slightly higher than that indicated in the simulation, although the qualitative nature of the two distributions is in general agreement. The experimental pressure distributions observed on the forward portion of the sidewall indicate a higher pressure rise, again consistent with perhaps a slightly higher Mach number felt at that position.

COMPARISON OF EXPERIMENTAL AND NUMERICAL SURFACE PRESSURE DISTRIBUTIONS (U)

M_∞ = 17.7 6° Sidewalls GCR = 5.0 Wedge Case

Sidewall Centerline

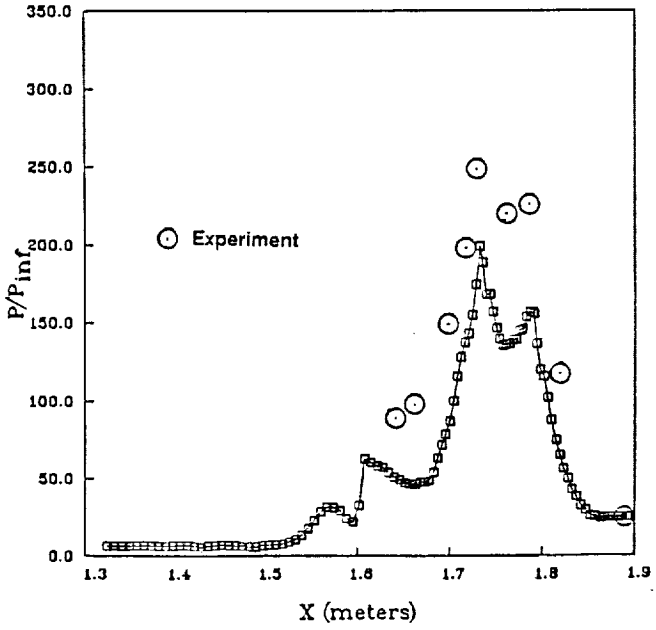

This figure shows the pressure distribution along the cowl center line. The overall pressure observed near the cowl lip is again approximately 1500 times that of the freestream, in good agreement with the simulation for this geometry for the freestream case as discussed previously.

NUMERICAL SURFACE PRESSURE DISTRIBUTIONS (U)

M_∞ = 17.7 6° Sidewalls GCR = 5.0 Wedge Case

Cowl Centerline

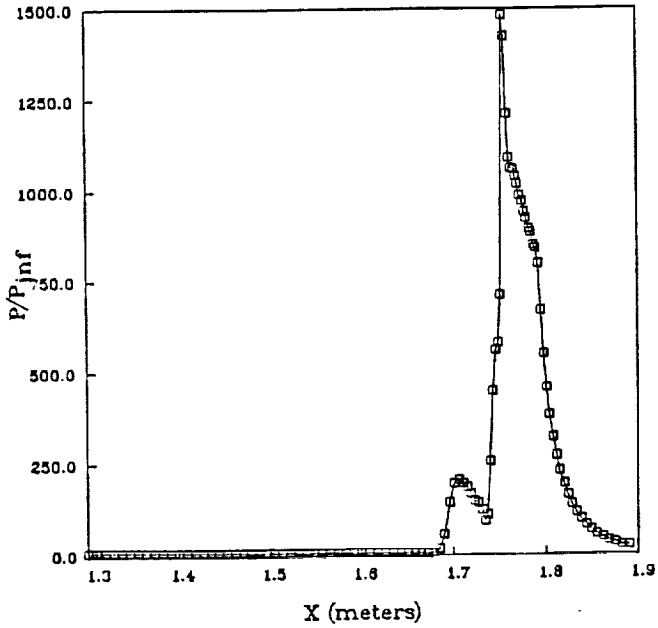

This figure shows the distribution of the product of the fluid density and streamwise velocity contours obtained on the vertical center plane within the inlet. The rather large values (indicated by the lighter, closely packed contours) of this parameter (which is related to the amount of fuel that can be burned), are rather disturbing and indicate over an order of magnitude variation across the inlet. This is consistent with the rather high pressures observed in the cowl and the low momentum content of the ramp boundary layer.

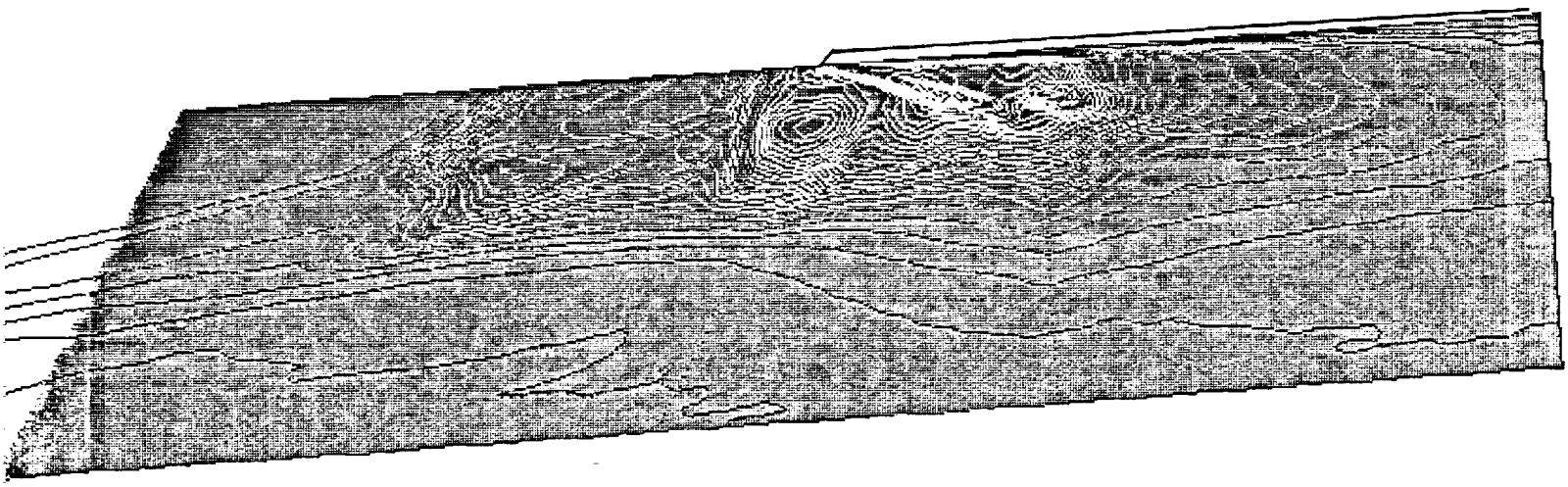

This figure shows contours of the product of density and streamwise velocity at three representative cross flow planes, one at the entrance to the inlet, one at the entrance to the constant area throat and one just upstream of the exit of the constant area throat. Again, the lighter regions near the cowl surface indicate a highly distorted flow represented by this parameter.

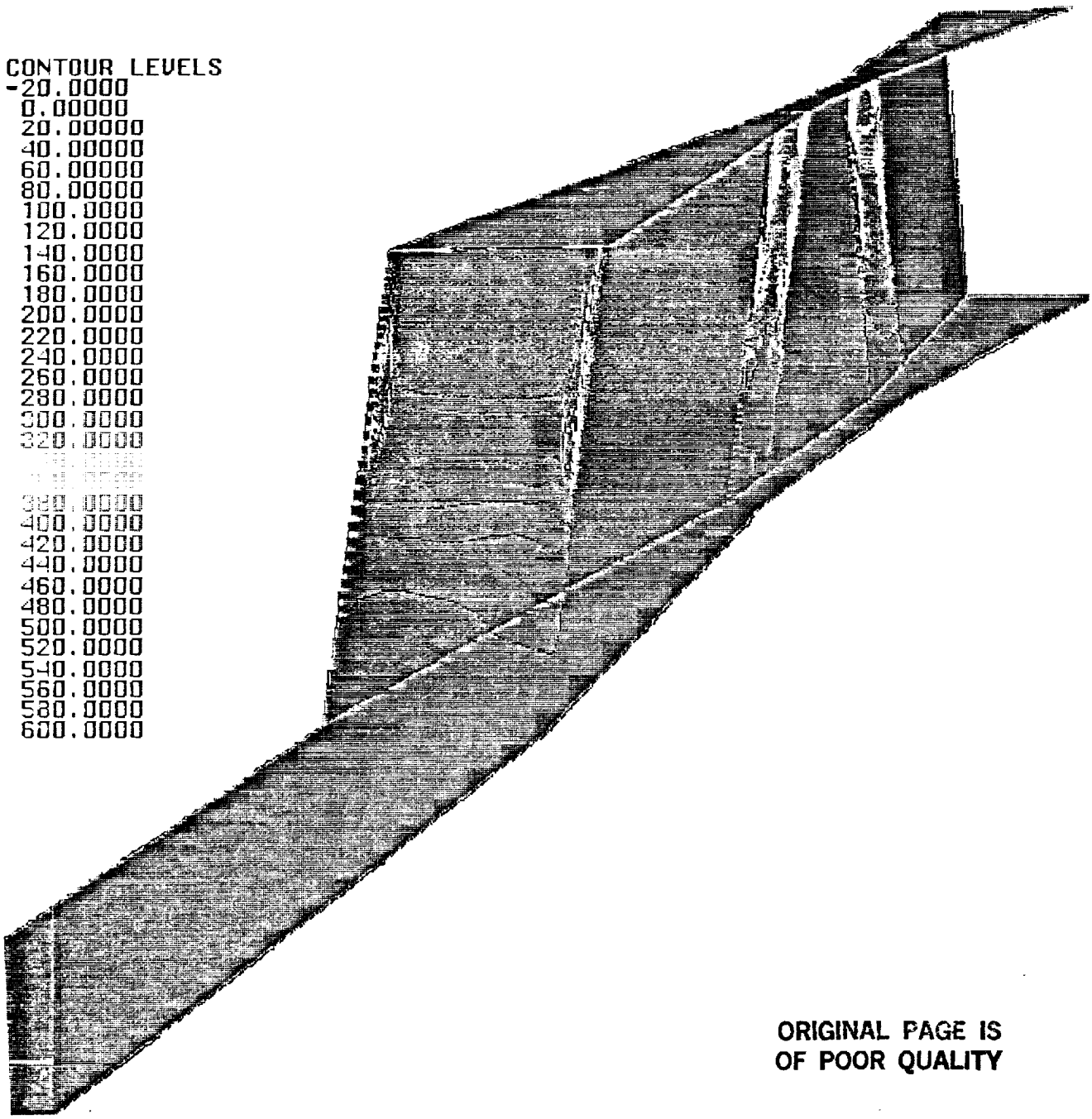

ORIGINAL PAGE IS
OF POOR QUALITY

Performance parameters are easily extracted from the numerical simulations and are presented in this figure for comparison in an attempt to highlight the effect of the presence of the entering boundary layer on inlet performance. Two cases, noted as freestream and boundary layer on this figure, are summarized for three parameters, the kinetic energy efficiency, the total pressure recovery in the absence of a normal shock wave, and the actual captured inlet mass flow. It is instructive to initially examine the mass averaged total pressure recovery. For the freestream case the value is .026, while for the entering boundary layer case the value is observed to be almost 10 times as large at 0.22. The explanation for this is related to the hypersonic viscous interaction occurring for the freestream case in which highly curved and steep oblique shock waves from the sidewall system are observed and are taken at the freestream Mach number of 21.6, while for the entering boundary layer case two additional, milder oblique shock waves occur. Initially the planar shock wave formed by the 4 degree wedge occurs and the inlet entrance Mach number is lower. These two factors are enhanced by the compression shock wave (discussed in previous figures) that reduces the Mach number through another oblique shock wave to a Mach number below 8. These differences alone are enough to account for the wide variation in total pressure recovery. Due to the compression of the flow across the initial wedge shock wave, a substantial increase in the unit mass flux approximately equal to 6 times that in the freestream produces a much higher mass flow, although the reduced freestream total pressure (from 2,000 at 21.6 to 1,000 at 17.7) drops the mass flow such that the net change is approximately 2-1/2 times that observed when the inlet is running in the freestream. Changes in kinetic energy efficiency reflective of the more efficient compression process for the boundary layer case indicates an increase from .980 to .985.

EFFECT OF ENTERING BOUNDARY LAYER ON PERFORMANCE (U)

	KINETIC ENERGY EFFICIENCY	TOTAL PRESSURE RECOVERY (No Normal Shock)	MASS FLOW Kg/s
FREESTREAM	0.980	0.026	0.031
BOUNDARY LAYER	0.985	0.220	0.080

CONCLUSIONS (U)

(U) NUMERICAL SIMULATIONS SHOW HIGHLY THREE-DIMENSIONAL FLOW FIELDS IN SWC INLETS.

(U) LARGE DISTORTIONS PREDICTED FOR BOTH FREESTREAM AND WEDGE CASES.

(U) CODE SIMULATES MANY FEATURES OF THE EXPERIMENTS

- LARGE STEADY SEPARATIONS PRESENT IN ALL CASES.
- ADDITIONAL OBLIQUE WAVE FOR WEDGE CASE.
- NO UNSTART ON WEDGE FOR ALL EXPERIMENTAL COWL POSITIONS.
- STRONG HYPERSONIC VISCOUS INTERACTION FOR FREESTREAM CASE.
- UNSTART FOR FREESTREAM CASE WITH COWL FORWARD.
- QUALITATIVE AGREEMENT WITH MOST SURFACE PRESSURES.

(U) ...BUT NOT ALL:

- UNSTART DETAILS DIFFER FOR FREESTREAM CASE.
- EXTENT OF SEPARATION DETAILS DIFFER.
- DETAILS OF OVERALL PRESSURE RISES DIFFER.

(U) CONTINUED NEED FOR DETAILED EXPERIMENTAL DATA IN THIS CLASS OF INLET TO PROVIDE A BASIS FOR MODELING IMPROVEMENT.